UC Berkeley

UC Berkeley Previously Published Works

Title

Large cells activate global protein degradation to maintain cell size homeostasis

Permalink

https://escholarship.org/uc/item/6vt3m79d

Author

Mark, Kevin

Publication Date

2021-11-11

DOI

10.1101/2021.11.09.467936

Copyright Information

This work is made available under the terms of a Creative Commons Attribution License, availalbe at https://creativecommons.org/licenses/by/4.0/

eScholarship.org Powered by the California Digital Library
University of California

bioRxiv preprint doi: https://doi.org/10.1101/2021.11.09.467936; this version posted November 11, 2021. The copyright holder for this preprint (which was not certified by peer review) is the author/funder, who has granted bioRxiv a license to display the preprint in perpetuity. It is made available under aCC-BY-NC-ND 4.0 International license.

Large cells activate global protein degradation to maintain cell size homeostasis

Shixuan Liu[1,2,3*,#], Ceryl Tan[1,2,*], Chloe Melo-Gavin[1,2], Kevin G. Mark[4], Miriam B. Ginzberg[2], Ron Blutrich[1,2], Nish Patel[2], Michael Rape[4], Ran Kafri[1,2,#]

Affiliations

[1]Department of Molecular Genetics, University of Toronto, Toronto, ON M5G 1A8, Canada
[2]Cell Biology, The Hospital for Sick Children, Toronto, ON M5G 0A4, Canada
[3]Chemical and Systems Biology, Stanford University, Stanford, CA 94305, USA
[4]Department of Molecular Cell Biology, University of California at Berkeley, Berkeley, CA 94720, USA
*equal contributions
[#]Correspondence: ran.kafri@sickkids.ca; shixuan@stanford.edu

Abstract

Proliferating animal cells maintain a stable size distribution over generations despite fluctuations in cell growth and division size. This tight control of cell size involves both cell size checkpoints (e.g., delaying cell cycle progression for small cells) and size-dependent compensation in rates of mass accumulation (e.g., slowdown of cellular growth in large cells). We previously identified that the mammalian cell size checkpoint is mediated by a selective activation of the p38 MAPK pathway in small cells. However, mechanisms underlying the size-dependent compensation of cellular growth remain unknown. In this study, we quantified global rates of protein synthesis and degradation in naturally large and small cells, as well as in conditions that trigger a size-dependent compensation in cellular growth. Rates of protein synthesis increase proportionally with cell size in both perturbed and unperturbed conditions, as well as across cell cycle stages. Additionally, large cells exhibit elevated rates of global protein degradation and increased levels of activated proteasomes. Conditions that trigger a large-size-induced slowdown of cellular growth also promote proteasome-mediated global protein degradation, which initiates only after growth rate compensation occurs. Interestingly, the elevated rates of global protein degradation in large cells were disproportionately higher than the increase in size, suggesting activation of protein degradation pathways. Large cells at the G1/S transition show hyperactivated levels of protein degradation, even higher than similarly sized or larger cells in S or G2, coinciding with the timing of the most stringent size control in animal cells. Together, these findings suggest that large cells maintain cell size homeostasis by activating global protein degradation to induce a compensatory slowdown of growth.

Keywords

cell size; cell size homeostasis; growth rate regulation; compensatory growth; protein degradation

bioRxiv preprint doi: https://doi.org/10.1101/2021.11.09.467936; this version posted November 11, 2021. The copyright holder for this preprint (which was not certified by peer review) is the author/funder, who has granted bioRxiv a license to display the preprint in perpetuity. It is made available under aCC-BY-NC-ND 4.0 International license.

Introduction

To maintain the homeostasis of cell size, proliferating cells double their mass from one division to the next and divide into similarly sized daughter cells. This stringent regulation of cell size exists in wide-ranging systems such as single-celled yeasts (Hartwell et al., 1974; Johnston et al., 1977; Nurse, 1975; Schmoller et al., 2015), animal cells in culture and within tissues (Ginzberg et al., 2018; Liu et al., 2018; Xie and Skotheim, 2020; Zatulovskiy et al., 2020), as well as plant meristem cells (D'Ario et al., 2021; Serrano-Mislata et al., 2015). Misregulation of cell size control results in increased size heterogeneity, which is typically observed during neoplastic growth and is a hallmark of malignancy in many tumors, including breast cancer and small cell lung cancer (Asadullah et al., 2021; Bell and Waizbard, 1986; Ginzberg et al., 2015; Lee et al., 1992).

How is cell size controlled and how does cellular growth in mass coordinate with the cell cycle program? A major mechanism is the cell size checkpoint, which hinders cell cycle progression for cells that are smaller than the target size. The mammalian G1/S cell size checkpoint was first reported by Zetterberg and Killander over 50 years ago (Killander and Zetterberg, 1965; Zetterberg and Killander, 1965). Subsequently, similar size checkpoints have been identified in single-celled yeasts (Hartwell et al., 1974; Nurse, 1975). In recent years, the functioning of cell size checkpoints has been investigated with increasingly powerful technologies (Cadart et al., 2018; D'Ario et al., 2021; Liu et al., 2018; Schmoller et al., 2015; Varsano et al., 2017; Xie and Skotheim, 2020). With increased resolution, these newer studies directly confirmed that smaller cells spend longer periods of growth in G1, allowing cells to reach the target size as they transition into S phase. Although it is not yet clear how animal cells sense their size, studies have revealed roles for both the p38 MAPK (Liu et al., 2018; Sellam et al., 2019) and the CDK4/Rb pathways (Tan et al., 2021; Zatulovskiy et al., 2020).

In addition to cell size checkpoints, two recent studies on mammalian cell size control suggest that cells also employ size-dependent regulation of cellular growth rate (Cadart et al., 2018; Ginzberg et al., 2018). Authors of the studies used different methods to measure the growth of individual cell size throughout the cell cycle and found that the rate of cell growth negatively correlated with cell size at various cell cycle stages. Ginzberg et al. further applied chemical and genetic perturbations that slowed down or accelerated cell cycle progression and observed compensatory changes in the rate of cellular growth, which buffered the initial effect on cell size (**Fig. 1A**) (Ginzberg et al., 2018). For example, cells under CDK2 inhibition were forced to grow for a longer period in G1, resulting in an immediate increase in cell size. Remarkably, cells later compensated for this perturbation with a reduced rate of mass accumulation, resulting in only a small increase in cell size (**Fig. 1B-C**). To discriminate this mechanism from *size checkpoints*, we use the term *cell size-dependent compensatory growth* (or *compensatory growth*). Notably, this compensation does not occur with CDK4/6 inhibition (Ginzberg et al., 2018), which was found to reprogram cells to a larger target size (see (Tan et al., 2021)). Altogether, these studies suggest that cells can "sense" their size to regulate not only cell cycle progression (e.g., cell cycle checkpoints), but also adapt the cell growth program to maintain cell size homeostasis.

bioRxiv preprint doi: https://doi.org/10.1101/2021.11.09.467936; this version posted November 11, 2021. The copyright holder for this preprint (which was not certified by peer review) is the author/funder, who has granted bioRxiv a license to display the preprint in perpetuity. It is made available under aCC-BY-NC-ND 4.0 International license.

What are the mechanisms of this size-dependent regulation of cell growth? The rate of macromolecular growth depends on the interplay between the biosynthesis and degradation of proteins, lipids, polysaccharides, and other macromolecules (Alber and Suter, 2019). In an actively proliferating mammalian cell, proteins represent more than half of the cell's total dry mass (Mitchison, 1971), and are under active turnover (Ghenim et al., 2021; Liu et al., 2020). Total protein content also linearly scales with the dry mass and volume of cells at different cell cycle stages (Berenson et al., 2019; Kafri et al., 2013). The balance between protein translation and degradation has been shown to significantly influence cell size in various cell types, including neurons, muscles, and cancer cells (Acebron et al., 2014; Franklin and Johnson, 1998; Gordon et al., 2013; Sandri, 2013), suggesting a vital role of protein homeostasis in cell size control.

In this study, we ask whether the size-dependent regulation of cellular growth is mediated by protein synthesis or protein degradation. We found that proteasome-mediated global protein degradation, rather than protein synthesis, underlies the *size-dependent compensatory growth* and functions in parallel with cell size checkpoints to promote cell size homeostasis (**Fig. 5**).

Results

A quantitative assay for the size-dependent regulation of cellular growth rate

To robustly trigger a compensatory slowdown of growth, we employed a CDK2 inhibitor assay that was developed by Ginzberg et al. (Ginzberg et al., 2018). In this assay, unsynchronized cell populations were treated with a low dose of the CDK2 inhibitor, SNS-032, to induce a longer G1 phase. We carefully optimized a concentration range that inhibits CDK2 function without arresting the cell cycle (**Fig. S1**). Cells were subsequently fixed at different timepoints and profiled for proliferation rate, cell size, and cell cycle stage. Cell size was measured with Alexa fluorophore-conjugated succinimidyl ester (SE), which reacts with primary amines and quantifies total protein content of the cell as previously described (Kafri et al., 2013; Mugahid et al., 2020; Neurohr et al., 2019). As shown in Ginzberg et al. (Ginzberg et al., 2018), although cell size initially increased for CDK2-inhibited cells as a result of the prolonged cell cycle, it gradually plateaus after ~24 hr (**Fig. 1B**). We inferred average rates of cell proliferation and cell growth from the dynamics of cell number and cell mass (see Methods). This revealed that CDK2-inhibited cells initially grew at the same rate as control but later, after 24 hr of treatment, compensated with a 24% reduced rate of mass accumulation (**Fig. 1C**). In comparison, rates of cell proliferation remained unchanged (25% lower than control) throughout the experiment (**Fig. 1C**) (Ginzberg et al., 2018). The delayed response in cellular growth rate suggests, as in Ginzberg et al., that the influence of CDK2 inhibitor on growth rate is indirect and is mediated by a property that accumulates over time, presumably cell size. These findings support the report that both the cell cycle and cell growth programs are part of a negative feedback circuit that maintains cell size homeostasis (Ginzberg et al., 2018).

To further investigate the robustness of the assay, we employed time-lapse imaging to directly quantify single cell dynamics of size growth. Using the nuclear area delineated by SiR-DNA as a proxy for cell size, we followed RPE1 cells stably expressing the degron of Geminin fused to a

bioRxiv preprint doi: https://doi.org/10.1101/2021.11.09.467936; this version posted November 11, 2021. The copyright holder for this preprint (which was not certified by peer review) is the author/funder, who has granted bioRxiv a license to display the preprint in perpetuity. It is made available under aCC-BY-NC-ND 4.0 International license.

monomeric Azami green (mAG-hGem) (Sakaue-Sawano et al., 2008) throughout ~60 hr of SNS-032 treatment. Consistent with results from the fixed cell assay, CDK2 inhibition resulted in a longer G1 phase (+3.5 hr, 32%) and lower growth rates of nuclear size (-21%) (**Fig. 1D-G**). Although CDK2-inhibited cells had a larger initial size as a result of prolonged growth duration from the previous cycle, they grew slower and became similarly sized as control cells around the G1/S transition, which was apparent when growth trajectories were computationally synchronized to the timing of their G1/S transition (**Fig. 1E**). These findings provide further evidence for the size-dependent compensation in cell growth. CDK2 inhibition induced prolonged growth duration and an initial increase in cell size, which is then compensated by a delayed response of reduced growth rate, affirming that cellular growth rate is adaptively regulated to maintain cell size homeostasis.

Compensatory changes in cellular growth rate are not regulated at the level of global protein synthesis

Because cell growth reflects the balance between rates of protein synthesis and protein degradation, we first asked whether the compensatory slowdown of growth is mediated through reduced rates of protein synthesis in large cells. We used a multiplex, single-cell labeling strategy to jointly profile overall protein synthesis rates, macromolecular protein mass, and cell cycle state in thousands of asynchronized proliferating cells. To quantify global translation rates, we performed kinetic pulse measurements with a derivatized methionine analog, L-azidohomoalanine (AHA) (Calve et al., 2016), which measures the amount of AHA that is incorporated into newly synthesized proteins. We performed an AHA pulse for 3 hours to obtain a high signal-to-noise ratio in a relatively short period of the cell cycle.

If the compensatory slowdown of growth is driven by slower rates of protein synthesis, larger cells should have lower rates of AHA incorporation. Our results, however, demonstrate the contrary. In unperturbed cells, AHA incorporation levels positively correlated with total protein content (R=0.91) (**Fig. 2A**), indicating a faster rate of protein synthesis in large cells. To test if the positive correlation between cell size and AHA incorporation is cell cycle dependent, we further segregated cells by their cell cycle stage and found that the dependence of AHA incorporation on size was consistent for G1, S, and G2 cells (**Fig. 2B**). Markedly, the linear dependence of AHA incorporation on cell size persists across a wide range of sizes, even for cells that are ~2 fold larger, as induced by CDK4/6 inhibition (**Fig. 2C**).

Because we did not observe a compensatory slowdown of AHA incorporation in naturally large cells, we next tested whether the compensatory slowdown of growth following CDK2 inhibition is regulated at the level of protein synthesis. We employed the same strategy described in **Fig. 1B** and additionally measured rates of AHA incorporation. CDK2-inhibited cells demonstrated a slight increase in both cell size (~11%) and AHA incorporation (~4%) compared to that of control (**Fig. 2C**), despite the compensatory slowdown of growth (**Fig. 1**). Consistent with measurements in unperturbed cells, CDK2-inhibited cells maintained a similar linear correlation between cell size and AHA incorporation, both at the single cell level and across different cell cycle stages (**Fig. 2B-C**), suggesting that the protein synthesis machinery is not affected by CDK2 inhibition throughout the duration of the experiment. Together, results from the AHA pulse

bioRxiv preprint doi: https://doi.org/10.1101/2021.11.09.467936; this version posted November 11, 2021. The copyright holder for this preprint (which was not certified by peer review) is the author/funder, who has granted bioRxiv a license to display the preprint in perpetuity. It is made available under aCC-BY-NC-ND 4.0 International license.

experiments suggest that the compensatory slowdown of growth in CDK2-inhibited cells is not mediated through a decrease in overall rates of protein synthesis but likely through an increase in overall protein degradation.

Large cells have more active proteasomes and higher rates of global protein degradation

To measure rates of protein degradation, we implemented a cycloheximide chase assay and quantified the loss of total protein mass over time. In this assay, protein synthesis was inhibited by cycloheximide; therefore, the loss of macromolecular protein mass reflected changes resulting from protein degradation. Interestingly, we observed significantly increased rates of protein degradation in larger cells (80th percentile), as compared to smaller cells (20th percentile) (**Figs. 3A, S2**), supporting the hypothesis that large cells may activate global protein degradation to initiate a compensatory slowdown of growth.

Proteasome-mediated protein degradation is a major route of protein turnover in non-starved cells (Lecker et al., 2006). The major targeting signal for proteasomal degradation is a post-translational modification involving ubiquitin chains linked through Lysine 48 (K48) (Yau and Rape, 2016).To further test whether larger cells undergo higher rates of proteasome-mediated degradation, we measured the turnover (i.e. clearance) of K48-linked polyubiquitinated proteins (K48-polyUb) in CDK2 inhibited cells that undergo a compensatory slowdown of growth. K48-polyUb turnover rates were quantified as the increase in intracellular pools of K48-polyUb that is caused by a 30 min treatment with a potent irreversible proteasome inhibitor, carfilzomib (CFZ). The excess amount of K48-polyUb in CFZ-treated cells compared to that of untreated cells, which we term ΔK48-polyUb, estimates the amount of K48-polyUb proteins that would have been degraded during the 30 min had the proteasome not been inhibited. Cell size and the partitioning of cells into different cell cycle stages were not significantly influenced by the 30 min treatment with CFZ (**Fig. S3**). Using this method, we measured the rates of proteasome-mediated protein degradation (ΔK48-polyUb) in CDK2-inhibited cells that were induced to undergo a compensatory slowdown of growth. CDK2-inhibited cells showed higher rates of ΔK48-polyUb, affirming an involvement of the proteasome in compensatory growth. The dependence of compensatory growth on proteasome activity is further supported by the temporal similarity of these two processes. Both the slowdown in growth rate and increase in ΔK48-polyUb showed delayed dynamics following CDK2 inhibition. CDK2-inhibited cells had similar ΔK48-polyUb as control during the first 8 hrs of treatment, but later showed a significant increase in ΔK48-polyUb at 24 hr, indicating increased rates of protein degradation (**Fig. 3B-C**). This increased turnover of K48-polyUb proteins coincides with the time frame at which CDK2-inhibited cells undergo compensatory changes in cellular growth rate (**Fig. 1B-C**). The delayed kinetics suggest that the increased ΔK48-polyUb is not triggered by the immediate inhibition of CDK2 activity but rather, from the buildup of excessive cell mass triggered by the slow and gradual influence of the longer cell cycle. Altogether, these results indicate that the compensatory slowdown of cell growth is mediated by increased clearance of K48-polyUb.

What mediates the size-dependent increase in proteasome-mediated protein degradation? One possibility is that large cells have more proteasomes. To test this, we compared the proteasome content in control and CDK2-inhibited cells by probing the 20S proteasome subunit β5, PSMB5

bioRxiv preprint doi: https://doi.org/10.1101/2021.11.09.467936; this version posted November 11, 2021. The copyright holder for this preprint (which was not certified by peer review) is the author/funder, who has granted bioRxiv a license to display the preprint in perpetuity. It is made available under aCC-BY-NC-ND 4.0 International license.

(Russell et al., 1999). These measurements revealed that CDK2-inhibited cells had a similar level of proteasomes per unit mass as control (**Fig. 3D, S4**), suggesting a small increase in total proteasome content for the CDK2-inhibited cells, proportional to the increase in cell size. Another possibility is that large cells may activate more proteasomes. It was reported that a fraction of the intracellular proteasomes are catalytically inactive and can be stimulated in response to stress (Collins and Goldberg, 2017; Livneh et al., 2016). To quantify the levels of active proteasomes in single cells, we used a proteasome activity probe, MV151. MV151 is a fluorescent and cell-permeable proteasome inhibitor that selectively binds to the catalytic core of active proteasomes and provides fluorescence readouts of active proteasomes at single cell resolution (Verdoes et al., 2006). These measurements revealed a significant positive correlation between cell size and levels of active proteasomes ($R=0.904$, $p<0.01$), suggesting that large cells may also have higher proteasome activation (**Fig. 3E**). As a positive control, the proteasome inhibitor, bortezomib, eliminated the dependence of active proteasomes on cell size. Together, these findings suggest that the higher rates of protein degradation in large cells are mediated by both increased levels of ubiquitinated proteins and a higher percentage of active proteasomes.

Large cells have higher rates of protein degradation per unit cellular mass

Our findings suggest that larger cells have higher rates of protein synthesis as well as higher rates of protein degradation. A simple interpretation of these data would posit that both the rates of protein synthesis and degradation linearly scale with cell size. For example, a cell that increased 50% in size would have a 50% increase in both the rates of protein synthesis and degradation. To examine this quantitative relationship, we calculated fold changes in protein synthesis and degradation as a function of fold changes in cell size. Perturbation of CDK2 activity promotes proportional increases in both cell size and the rate of AHA incorporation across all cell cycle stages (**Fig. 2C**). However, cell size-dependent changes in protein degradation (ΔK48-polyUb) are disproportionately larger in CDK2-inhibited cells. On average, ΔK48-polyUb increased ~32% in CDK2-inhibited cells, whereas cell size increased ~15% compared to control (**Fig. 3F**). Similar disproportionate increases in protein degradation existed across all interphase stages (G1: 44%, S: 42%, G2: 31%) (**Fig. 3F**). These results highlight a contrast between the cell size dependency of protein synthesis and protein degradation. Whereas larger cells have higher rates of protein synthesis, the rates of AHA incorporation per unit cell mass do not significantly vary when comparing cells of different sizes. By contrast, larger cells have higher rates of protein degradation even when quantified per unit cellular mass, suggesting an activation of protein degradation in large cells, in addition to large cells having more proteins to degrade.

Large cells at the G1/S transition show hyperactive global protein degradation

We next examined the cell cycle dependency of the increased global protein degradation observed in large cells by comparing ΔK48-polyUb for cells at different cell cycle stages. Throughout G1, S, and G2 phases, cells under 24 hr of CDK2 inhibition showed significantly higher levels of ΔK48-polyUb compared to cells under control conditions (**Fig. S5**), implicating a sustained activation of protein degradation in cells that undergo compensatory slowdown in

bioRxiv preprint doi: https://doi.org/10.1101/2021.11.09.467936; this version posted November 11, 2021. The copyright holder for this preprint (which was not certified by peer review) is the author/funder, who has granted bioRxiv a license to display the preprint in perpetuity. It is made available under aCC-BY-NC-ND 4.0 International license.

cellular growth. Strikingly, when compared across cell cycle stages, cells at the G1/S transition displayed the highest level of ΔK48-polyUb for both control and CDK2-inhibited cells (**Fig. 4A-B**). Notably, rates of global protein degradation observed in these large cells at the G1/S transition were higher than even those of similarly sized or larger cells in S and G2. Together, these results suggest a hyperactivation of global protein degradation at the G1/S transition.

To further investigate the cell cycle dependency of compensatory growth, we performed pseudo-time trajectory analysis and aligned cells to a continuous cell cycle axis using their DNA content and the FUCCI cell cycle marker mAG-hGem (**Fig. 4C**, see Methods) (Kafri et al., 2013) This allows the extraction of average cellular dynamics from single cell snapshots of fixed steady-state populations. Interestingly, these measurements revealed a subpopulation of exceedingly large cells at the G1/S transition, with sizes that are comparable to or often larger than S and G2 phase cells (**Fig. 4D**). We confirmed through time-lapse imaging that similarly large cells at the G1/S transition were not arrested but continued to progress through the cell cycle (**Fig. S6A**). These large cells at the G1/S transition also demonstrated the highest levels of ΔK48-polyUb per unit mass (**Fig. 4E**), indicating a state of hyperactive protein degradation specifically for large G1/S cells.

To further test this observation, we used time-lapse imaging and examined the changes in cellular growth rate caused by the inhibition of protein synthesis for cells before and after the G1/S transition. We applied partial mTOR inhibition and separately measured cellular growth rate for small and large cells. In control conditions, large cells on average grew faster in size than small cells, both before and after the G1/S transition (**Fig. S7A**), as a result of the overall faster rates of protein synthesis in large cells (**Fig. 2**). By contrast, cellular growth rates under mTOR inhibition became comparable for small and large cells before the G1/S transition but not after (**Fig. S7A**). This is despite rates of protein synthesis (AHA incorporation) decreasing proportionally for all cells (i.e., large cells continued to synthesize proteins faster than small cells) (**Fig. S7B**). These results suggest that large cells before the G1/S transition had higher rates of protein degradation, which balanced their higher protein synthesis rates, supporting our findings that large cells undergo hyperactivated protein degradation before entering S phase.

Taken together, our results demonstrate that large cells exhibit elevated rates of protein degradation throughout interphase, and that extremely large cells at the G1/S transition show hyperactivated levels of protein turnover. This mechanism can function collaboratively with the cell size checkpoints to promote cell size uniformity for both large and small cells.

Discussion

Cell size is fundamental to cellular physiology as it sets the scale for subcellular compartments, biosynthetic capacity, and cellular function. Evidence of cell size control has been reported from single-celled yeasts to multicellular animals and plants (Dolznig et al., 2004; Hartwell et al., 1974; Neufeld et al., 1998; Nurse, 1975; Willis et al., 2016; Xie and Skotheim, 2020; Zetterberg and Killander, 1965). The precision with which size is controlled also manifests in the cell size regularity observed in healthy tissues. In contrast, deregulation of size control often signals

bioRxiv preprint doi: https://doi.org/10.1101/2021.11.09.467936; this version posted November 11, 2021. The copyright holder for this preprint (which was not certified by peer review) is the author/funder, who has granted bioRxiv a license to display the preprint in perpetuity. It is made available under aCC-BY-NC-ND 4.0 International license.

cancerous growth as many tumors display increased heterogeneity in cell size (Asadullah et al., 2021; Bell and Waizbard, 1986; Lee et al., 1992).

Previous studies on cell size control have mostly focused on cell size checkpoints, in that a critical size threshold is required for cell cycle progression (D'Ario et al., 2021; Ginzberg et al., 2018; Liu et al., 2018; Sellam et al., 2019; Zatulovskiy et al., 2020). In this study, we investigated size-dependent compensatory growth, a cell size control mechanism that does not involve cell cycle checkpoints. To trigger compensatory growth, we promoted longer cell cycle periods by CDK2 inhibition, which resulted in an initial increase in cell size, followed by a delayed compensatory slowdown of growth (**Fig. 1**). We found that rates of global protein synthesis and degradation increase with cell size in both perturbed and unperturbed conditions (**Figs. 2-3**). Interestingly, although rates of protein synthesis remained proportional to cell size, rates of protein degradation were disproportionately higher in large cells (i.e., higher rates of protein degradation per unit mass), suggesting the activation of protein degradation pathways that are likely mediated by an increase in the total active proteasomes (**Fig. 3D-E**). In CDK2-inhibited cells, we observed a delayed activation of proteasome-mediated protein degradation that accompanied the compensatory slowdown of growth (**Fig. 1C, Fig. 3B-C**). We further compared these measurements across cell cycle stages and found that large cells at the G1/S transition demonstrate the highest increase in overall protein degradation (**Fig. 4**), consistent with the stringent size control observed at the G1 exit (Ginzberg et al., 2018; Zetterberg and Killander, 1965). These findings imply that the G1/S size checkpoint may also involve growth rate regulation. Based on these results, we propose a model whereby oversized cells achieve size homeostasis by activating global protein degradation through the proteasome pathway to compensate with a slower cell growth (**Fig. 5**).

In this study, we showed that large cells adaptively slow down their cell growth by activating global protein degradation. Previous work suggests that small cells may also adaptively accelerate their cell growth at certain periods of the cell cycle (Cadart et al., 2018; Ginzberg et al., 2018). This poses an intriguing possibility that small cells attain their target size by two complementary processes: a decrease in global protein degradation and a prolonged cell cycle, mediated by the cell size checkpoint. High-throughput screens on both animal cells and yeasts identified that small cells activate the stress-responding p38 MAPK (Hog1) pathway to prolong the cell cycle (Liu et al., 2018; Sellam et al., 2019). Interestingly, previous work on p38 found that activation of the pathway by osmotic stress results in reduced protein degradation and lower proteasome activity (Lee et al., 2010). In contrast, p38 inhibition significantly promoted proteasome activity (Leestemaker et al., 2017). It will be interesting to explore in future studies whether small cells reduce protein degradation to achieve their target size and whether this process is mediated by p38 MAPK.

Our data implies hyperactivated rates of global protein degradation in cells at the G1/S transition, specifically for the exceptionally large cells (**Fig. 4, Fig. S7**). These results suggest that in addition to accommodating cell size checkpoints, the G1/S transition may be a particularly important stage for global protein degradation and growth rate control, which further contributes to the homeostatic regulation of cell size. These findings are consistent with

bioRxiv preprint doi: https://doi.org/10.1101/2021.11.09.467936; this version posted November 11, 2021. The copyright holder for this preprint (which was not certified by peer review) is the author/funder, who has granted bioRxiv a license to display the preprint in perpetuity. It is made available under aCC-BY-NC-ND 4.0 International license.

previous work that identified decreases in the variability of both cell size and growth rate at the G1/S transition (Ginzberg et al., 2018; Kafri et al., 2013; Son et al., 2012; Zetterberg and Killander, 1965). It is well established that progression through the cell cycle, including the G1/S and G2/M transitions, is controlled by ubiquitination-mediated degradation of cell cycle regulators (Barr et al., 2016; Nakayama and Nakayama, 2006). It will be important to identify the enzymes responsible for the observed increase in K48-linked polyubiquitination in larger cells during the G1/S transition, as this may reveal whether compensatory degradation and cyclin turnover are mediated by the same, or separate, factors.

In this work, we identified a size-dependent regulation of global protein degradation without examining the identity of the degraded proteins. Do large cells selectively degrade certain proteins more than others? One way to approach this is to perform dynamic isotopic labeling and quantitative proteomics. Two recent studies (Cheng et al., 2021; Lanz et al., 2021) used such an approach and measured individual protein concentrations in cells of different sizes. Proteasome subunits were found at higher concentrations in large cells, consistent with elevated rates of ubiquitylation and protein turnover. Interestingly, components involved in translation show slightly reduced concentrations in large cells. Previous work in yeast (Neurohr et al., 2019) also demonstrated that oversized cells show impaired gene expression. If translation integrity is disrupted in large cells, increased levels of ubiquitin-mediated degradation may be required for the clearance of aberrant nascent polypeptides through protein quality control pathways.

Our findings provide mechanistic insight into the process of compensatory growth which, unlike cell size checkpoints, can be employed in the homeostatic size control of non-proliferating cells. This is an area of study that is sparsely explored but is of great importance. Most of the cells in an adult body are terminally differentiated and have ceased to proliferate; thus, size-dependent modulation of growth rate may potentially be the primary mechanism for their cell size control. Maintaining cells within their target size range is optimal for cellular and organ function. In adipocytes, the release of fatty acid induced by epinephrine was found to be highly dependent on the cell surface area (Zinder and Shapiro, 1971). Pancreatic beta cells undergoing hypertrophy show enhanced insulin secretion and improved glucose homeostasis *in vivo* (Helman et al., 2016). Across tissue types, cells dynamically control their size to modulate cell and tissue level functions in response to physiological demand; these include compensatory hypertrophy in pancreatic and hepatic cells (Dhawan et al., 2007; Ginzberg et al., 2015; Miettinen et al., 2014), compensatory renal cell hypertrophy following nephrectomy (Rojas-Canales et al., 2019) or increased urine flow (Boehlke et al., 2010), and the likely regulation of functional mass of the hormone-secreting glands in response to stress (Karin et al., 2020, 2021). These examples highlight the importance of cell size control in non-proliferating, differentiated cells. The experimental pipeline used in this study can be adapted to assess the roles of protein synthesis and degradation in non-proliferating cells, whether certain mechanisms are shared between proliferating and non-proliferating cells, and how these processes affect cellular functions.

bioRxiv preprint doi: https://doi.org/10.1101/2021.11.09.467936; this version posted November 11, 2021. The copyright holder for this preprint (which was not certified by peer review) is the author/funder, who has granted bioRxiv a license to display the preprint in perpetuity. It is made available under aCC-BY-NC-ND 4.0 International license.

Acknowledgements

We thank Yifat Merbl, Mikael Björklund, and members of the Kafri laboratories for helpful discussions. This work is supported by the Natural Sciences and Engineering Research Council of Canada (RGPIN-2015-05805) to R.K, the Restracomp Graduate and Postdoctoral Fellowship from the Research Training Center at the Hospital for Sick Children to S.L and M.B.G., the University of Toronto Open Fellowship to C.T., and the National Institute of General Medical Sciences of the National Institutes of Health award F32GM120956 to K.G.M.

Author Contributions

S.L. and R.K. conceived the study. S.L., C.T., K.G.M., C.M.G., M.B.G., R.B., N.P., and M.R. designed, performed, and analyzed the experiments. S.L. and C.T. wrote the manuscript with input from R.K., K.G.M., C.M.G., M.R., and N.P..

Declaration of Interests

The authors declare no competing interests.

bioRxiv preprint doi: https://doi.org/10.1101/2021.11.09.467936; this version posted November 11, 2021. The copyright holder for this preprint (which was not certified by peer review) is the author/funder, who has granted bioRxiv a license to display the preprint in perpetuity. It is made available under aCC-BY-NC-ND 4.0 International license.

Methods

Materials

This study did not generate new unique reagents. All chemical inhibitors were purchased from Selleckchem (SNS-032, S1145; Palbociclib, S4482; Bortezomib, S1013; Cycloheximide, S7418). Click-IT® L-azidohomoalaine was purchased from Thermo Scientific (C10102). The activity-based active proteasome probe (ABP) MV151 Bodipy-TMR was a kind gift from the Florea Lab at Leiden University. The anti-ubiquitin K48-specific antibody (Clone Apu2.07) was a kind gift from Genentech.

Cell culture

Retinal pigmented epithelial (RPE1, ATCC, RRID:CVCL 4388) cell line stably expressing the degron of Geminin fused to Azami Green (mAG-hGem) were cultured in DMEM medium (Life Technologies) supplemented with 10% Fetal Bovine Serum (FBS, Wisent, Montreal, QC) at 37°C in a humidified atmosphere with 5% CO_2. Measurements were made when cells were 60–80% confluent, to avoid the effects of sparse or dense culture on cell growth and proliferation.

Fixation, staining, and imaging

Cells were fixed in 4% paraformaldehyde (Electron Microscopy Sciences, Hatfield, PA) for 10 min, followed by permeabilization in cold methanol at -20°C for 5 min. Cells were stained with 0.4 µg/mL Alexa Fluor 647 carboxylic acid, succinimidyl ester (SE-A647, Invitrogen A-20006) for 2 hrs at RT. The cellular integrated intensity of SE-A647 provides an accurate measure of total protein mass, which is proportional to a cell's dry mass (Kafri et al., 2013; Mugahid et al., 2020). DNA was stained with 1 µg/mL DAPI (Sigma D8417) for 10 min at RT. Cells were imaged using the Operetta High-Content Imaging System (PerkinElmer, Woodbridge, ON) at 20X magnification. Automated image processing was performed as previously described (Liu et al., 2018).

Time lapse microscopy and analysis

RPE1 cells with stable expression of H2B-mTurquoise and Geminin-mVenus were seeded in 96-well µclear microplates (Greiner Bio-one, Monroe, NC) and grown in the incubator for at least 6 hr prior to imaging. The cells were imaged using the Operetta High-Content Imaging System. During imaging, the plate was incubated in a live cell chamber (37°C, 5% CO2), and cells were grown in FluoroBrite DMEM supplemented with FBS, L-glutamine and Sodium Pyruvate. As the cells were previously cultured in regular DMEM and displayed suboptimal cell proliferation after switching to FluoroBrite DMEM, cells were grown in FluoroBrite medium for a period of 2 weeks to adapt to the new medium before the time lapse experiments. Widefield fluorescent images of H2B-mTurquoise and Geminin-mVenus were collected every 15 min at 20X magnification for 60 hr. Under this experimental setting, the microscope could support imaging of up to four wells. To track the movement and division of single cells, and analyze nuclear area dynamics and cell cycle progression, we used the same methods as described in Liu et al. (Liu et al., 2018). Growth rate is estimated as the first derivative of the smoothed nuclear area dynamics, and all measurements presented in the study only examined the cells tracked from one division to the

bioRxiv preprint doi: https://doi.org/10.1101/2021.11.09.467936; this version posted November 11, 2021. The copyright holder for this preprint (which was not certified by peer review) is the author/funder, who has granted bioRxiv a license to display the preprint in perpetuity. It is made available under aCC-BY-NC-ND 4.0 International license.

next. The first and last six time points of the cell cycle were removed from the growth rate analysis because of the influence of nuclear breakdown and formation.

Cell cycle stages

Cells were first partitioned, according to their integrated nuclear DNA level, into G1 (2N), S (2N-4N) and G2 (4N) phases. Progression through the G1 phase was further divided, based on the fluorescence of integrated nuclear Geminin, into early G1 (low baseline Geminin) and G1/S transition (higher Geminin). The thresholds were automatically detected based on the distributions of DNA and log(Geminin).

Measures of AHA incorporation

To quantify rates of nascent protein synthesis, cells were treated with the CDK4/6 inhibitor Palbociclib (50nM) or CDK2 inhibitor SNS-032 (25nM) for 48 hr, then pulse-labeled with Click-IT® L-azidohomoalanine (AHA, Invitrogen C10102) for 3 hr as described in the manufacturer's protocol. Cells were then fixed and stained for DAPI and SE-A647. Rates of AHA incorporation were determined by labeling the cells with Alexa Fluor® 488 DIBO alkyne (Invitrogen C10405), followed by imaging and quantification of the integrated intensity of the fluorophore on a single cell basis as detailed above. As a negative control, cells were treated with 1 µM of the protein synthesis inhibitor cycloheximide (CHX).

Cycloheximide chase experiment

RPE1-mAG-hGem cells were seeded at 1500 cells per well into 96-well Cell Carrier-96 ultra microplates (PerkinElmer, Woodbridge, ON) for at least 6 hr prior to treatment. The protein synthesis inhibitor cycloheximide (CHX) was then administered at 10µM for either 0, 1.5, 3, 6, or 9 hr. Cells were then fixed and stained for DAPI and SE-A647, and imaged as detailed above.

Total protein loss over time was measured for the smaller 20% (20^{th} percentile) and the larger 20% (80^{th} percentile) of G1, S, or G2 cells separately. Under this partition, large (80^{th} percentile) and small (20^{th} percentile) cells were also normalized to their respective initial cell mass by subtracting each time point by its cell mass at time 0.

Measurements of active proteasomes

RPE1-mAG-hGem cells were seeded at 1500 cells per well into 96-well Cell Carrier-96 ultra microplates (PerkinElmer, Woodbridge, ON) for at least 6 hr prior to treatment. The cells were then treated with 1 µM activity-based active proteasome probe (ABP) MV151 Bodipy-TMR for 2 hr. MV151 binds to the inside of the catalytic core (20S) of active proteasomes, providing a total fluorescence intensity (per cell) that is proportional to proteasomal activity (Verdoes et al., 2006). As a negative control, cells were treated with 1 µM of the proteasome inhibitor Bortezomib. Cells were then fixed and stained for DAPI and SE-A647, and imaged as detailed above.

bioRxiv preprint doi: https://doi.org/10.1101/2021.11.09.467936; this version posted November 11, 2021. The copyright holder for this preprint (which was not certified by peer review) is the author/funder, who has granted bioRxiv a license to display the preprint in perpetuity. It is made available under aCC-BY-NC-ND 4.0 International license.

Measurements of K48-polyUb turnover

RPE1-mAG-hGem cells were seeded at 1500 cells per well into 96-well Cell Carrier-96 ultra microplates (PerkinElmer, Woodbridge, ON) for at least 6 hr prior to treatment. Cells were then treated with 25nM SNS-032 or DMSO control (<0.5%v/v) for 1, 8, or 24 hr before fixation. 30 min before fixation, half of each condition were treated with a proteasome inhibitor (8 μM Carfilzomib, CFZ). After fixation, cells were immunostained for total levels of K48-linked polyubiquitin with a primary antibody against K48-polyUb chains (Clone Apu2.07, Genentech, 1:500) for 2 hrs at room temperature, followed by incubation with a secondary antibody (Goat anti-Human IgG (H+L) Cross-Adsorbed Secondary Antibody, Alexa 555, ThermoFisher, 1:500) for 30 min at room temperature. Cells were then stained for DAPI and SE-A647, and imaged as detailed above. For Fig. 4E, single cell measurements of K48-polyUb were normalized to cell size such that the heatmap depicts ΔK48-polyUb per unit mass.

Whole cell lysis and western blotting

To prepare whole cell lysates, cells were rinsed with ice-cold PBS and solubilized with RIPA Lysis Buffer (Boston Bio-Products, Boston MA) [50 mM Tris-HCl, 150 mM NaCl, 5 mM EDTA, 1 mM EGTA, 1% NP-40, 0.1% SDS and 0.5% sodium deoxycholate, pH 7.4] supplemented with protease and phosphatase inhibitor cocktail (Thermo Scientific, Burlington, ON). Protein concentration was determined using the BCA protein assay (Thermo Scientific, Burlington, ON). Proteins were suspended with 4X Bolt LDS Sample Buffer and 10X Bolt Reducing Agent and heated for 10 min at 70C. Samples of equal protein were resolved by SDS-polyacrylamide gel electrophoresis and subjected to immunoblotting for proteins as indicated. All western blot results in the figures have been reproduced in replicate experiments with cell lysates samples prepared in independent experiments.

Estimation of cell cycle length and growth rate from bulk measurements

Cells were treated with inhibitors on multiple 96-well plates and fixed every 20 hrs over a period of 3 days. The plate slated to be fixed on the last timepoint was imaged by digital phase contrast (Operetta High-Content Imaging System (PerkinElmer, Woodbridge, ON) every 12 hrs to acquire cell number estimates. Cell size was quantified using the total fluorescence intensity from SE-A647 at a single cell level. Growth rate and cell cycle length were quantified from population averages of cell size and cell number over time. To quantify cell cycle length (τ), we fit exponential curves to cell number over time ($N_t = N_0 e^{\alpha t}$), where N_t is the cell count at time t and $\alpha = \frac{ln(2)}{t}$. To estimate growth rate (ν), we calculated the rate of increase in bulk mass (M_t = *cell size x cell count*) of the total population and divided that by the cell number: $\nu = \frac{1}{Nt}\frac{dM}{dt}$. Due to our method of cell size measurement, growth rate quantifications were performed on fixed populations of cells.

Estimation of a continuous cell cycle axis

bioRxiv preprint doi: https://doi.org/10.1101/2021.11.09.467936; this version posted November 11, 2021. The copyright holder for this preprint (which was not certified by peer review) is the author/funder, who has granted bioRxiv a license to display the preprint in perpetuity. It is made available under aCC-BY-NC-ND 4.0 International license.

Single cell levels of DNA (DAPI) and Geminin (mAG-hGem) were reduced to a single variable (ℓ), which represents a continuous measure of cell cycle stages. See specific calculations in Kafri et al. (Kafri et al., 2013). In brief, the trajectory is detected as the probability density ridge in the DNA-Geminin distribution, and individual cells were projected to the trajectory through the shortest distance. Note the cell cycle trajectory detected in this study corresponds to an average progression over the cell cycle but does not necessarily reflect the relative duration of each phase.

bioRxiv preprint doi: https://doi.org/10.1101/2021.11.09.467936; this version posted November 11, 2021. The copyright holder for this preprint (which was not certified by peer review) is the author/funder, who has granted bioRxiv a license to display the preprint in perpetuity. It is made available under aCC-BY-NC-ND 4.0 International license.

Figures

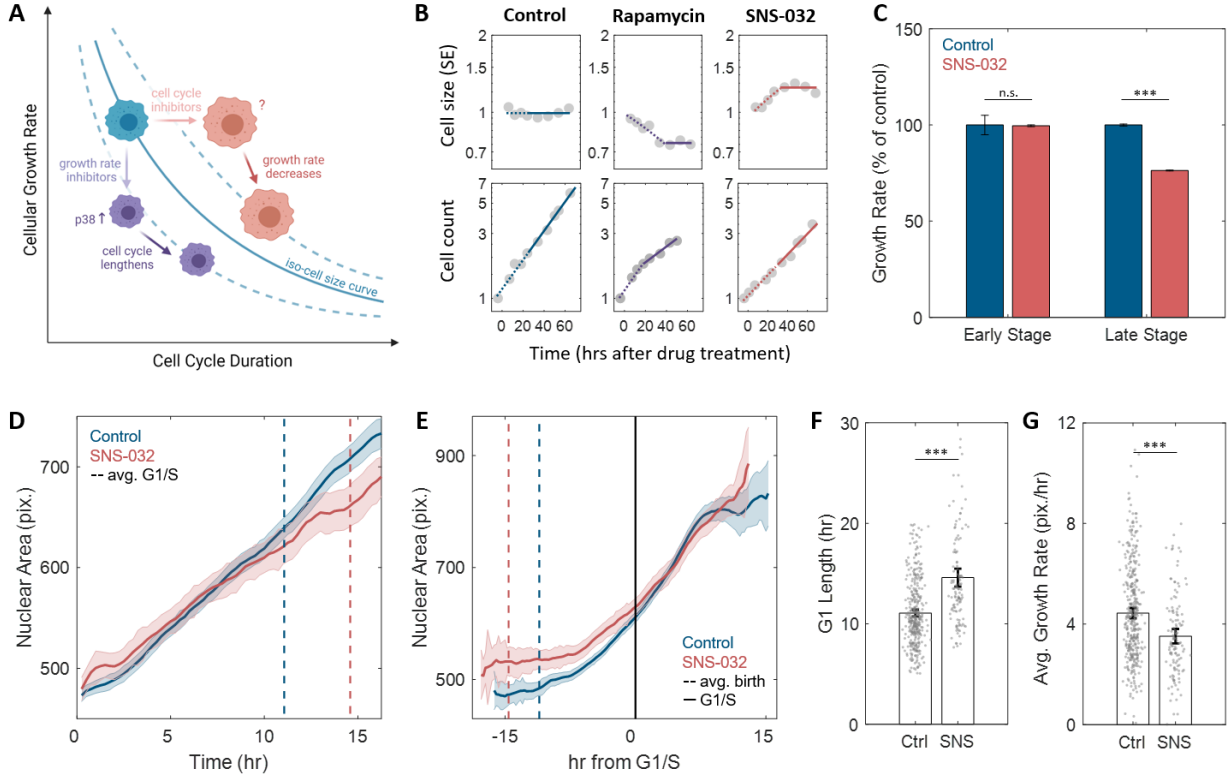

Figure 1. A quantitative assay for the size-dependent regulation of cellular growth rate. **(A)** Schematic showing the model of cell size control as described in Ginzberg et al. (Ginzberg et al., 2018). The solid blue line represents an iso-cell size curve: combinations of cellular growth rates (mass accumulation rates) and cell cycle length that result in the same cell size. The dashed blue lines represent iso-size curves at larger (upper curve) or smaller (lower curve) cell sizes. Perturbations that decrease cellular growth rate (e.g., mTOR inhibition) result in an initial decrease in cell size, followed by an adaptation involving the activation of p38 (Liu et al., 2018) to prolong the cell cycle, preventing further decrease in size (purple cells). Perturbations that lengthen the cell cycle (e.g., CDK2 inhibition) result in an initial increase in cell size, followed by a compensatory slowdown of growth that prevents further increase in cell size (red cells). **(B)** Measurements of average cell size with SE-A647 (top panel) and cell count (bottom panel) at different time points after treatment with the mTORC1 inhibitor rapamycin (70 nM) or CDK2 inhibitor SNS-032 (19 nM), supporting the model shown in (A). Y-axes are in log scale. Each cell size datapoint is an average from a population of >2000 cells. Values of cell size are normalized to control (0.1% v/v DMSO), such that the average cell size of control populations has the value of 1. Values of cell count are normalized to the cell number at the first time point. Dashed lines represent linear fitting of the early stage of each treatment, which is the time interval between drug addition and cell size stabilization (approximately one day). Solid lines represent linear fitting of the late stage, which is the time interval between cell size stabilization and the end of the experiment. **(C)** Estimated cellular growth rate for control or CDK2-inhibited cells presented as percent of control, estimated separately for early and late stages as indicated

bioRxiv preprint doi: https://doi.org/10.1101/2021.11.09.467936; this version posted November 11, 2021. The copyright holder for this preprint (which was not certified by peer review) is the author/funder, who has granted bioRxiv a license to display the preprint in perpetuity. It is made available under aCC-BY-NC-ND 4.0 International license.

in (B). Error bars represent 95% confidence intervals. (B-C) are reproductions of Fig. 6A and Fig. 6B from Ginzberg et al. (Ginzberg et al., 2018) to demonstrate the assay. **(D)** Average nuclear area as a function of time since division for control (0.1% v/v DMSO, N=365) and CDK2-inhibited cells (20 nM SNS-032, N=125), measured from live-cell imaging. Shaded regions mark 95% confidence intervals. Dashed lines mark the average time of G1/S transition for each condition. **(E)** Average nuclear area as a function of time with growth trajectories computationally synchronized to their time of G1/S transition (solid black line). Shaded regions mark 95% confidence intervals. Dashed lines mark the average time of birth/division for each condition. Note for D-E, CDK2-inhibited cells had larger initial sizes, progressed through G1/S later, and showed slower growth in size (shallower slope), compared to the control. **(F-G)** Bar plot with single cell data comparing the **(F)** G1 length and **(G)** average growth rate of size for control and SNS-032-treated cells. Bar height represents mean, error bar represents 95% confidence intervals. ***p<0.001 from two-sample t test.

bioRxiv preprint doi: https://doi.org/10.1101/2021.11.09.467936; this version posted November 11, 2021. The copyright holder for this preprint (which was not certified by peer review) is the author/funder, who has granted bioRxiv a license to display the preprint in perpetuity. It is made available under aCC-BY-NC-ND 4.0 International license.

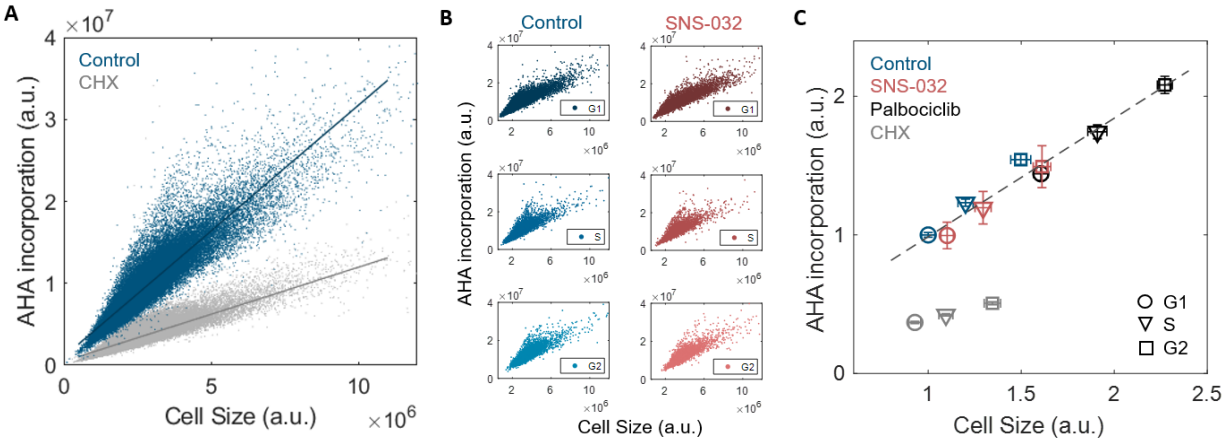

Figure 2. Global rates of protein synthesis scale with cell size.
(A) Single cell measurements of global protein synthesis rates (AHA incorporation) as a function of cell size for control (0.1% v/v DMSO) and cycloheximide (3 μM CHX)-treated cells. Lines show linear fit. **(B)** Single cell measurements of AHA incorporation as a function of cell size for G1, S, or G2 cells under control or CDK2 inhibition (25 nM SNS-032). **(C)** Median rates of protein synthesis for G1, S, or G2 control cells or under 25 nM SNS-032, 50 nM palbociclib, or 3 μM cycloheximide treatment. Data presented as fold-change over G1 cells of control, with error bars indicating ± 95% confidence interval, n=10.

bioRxiv preprint doi: https://doi.org/10.1101/2021.11.09.467936; this version posted November 11, 2021. The copyright holder for this preprint (which was not certified by peer review) is the author/funder, who has granted bioRxiv a license to display the preprint in perpetuity. It is made available under aCC-BY-NC-ND 4.0 International license.

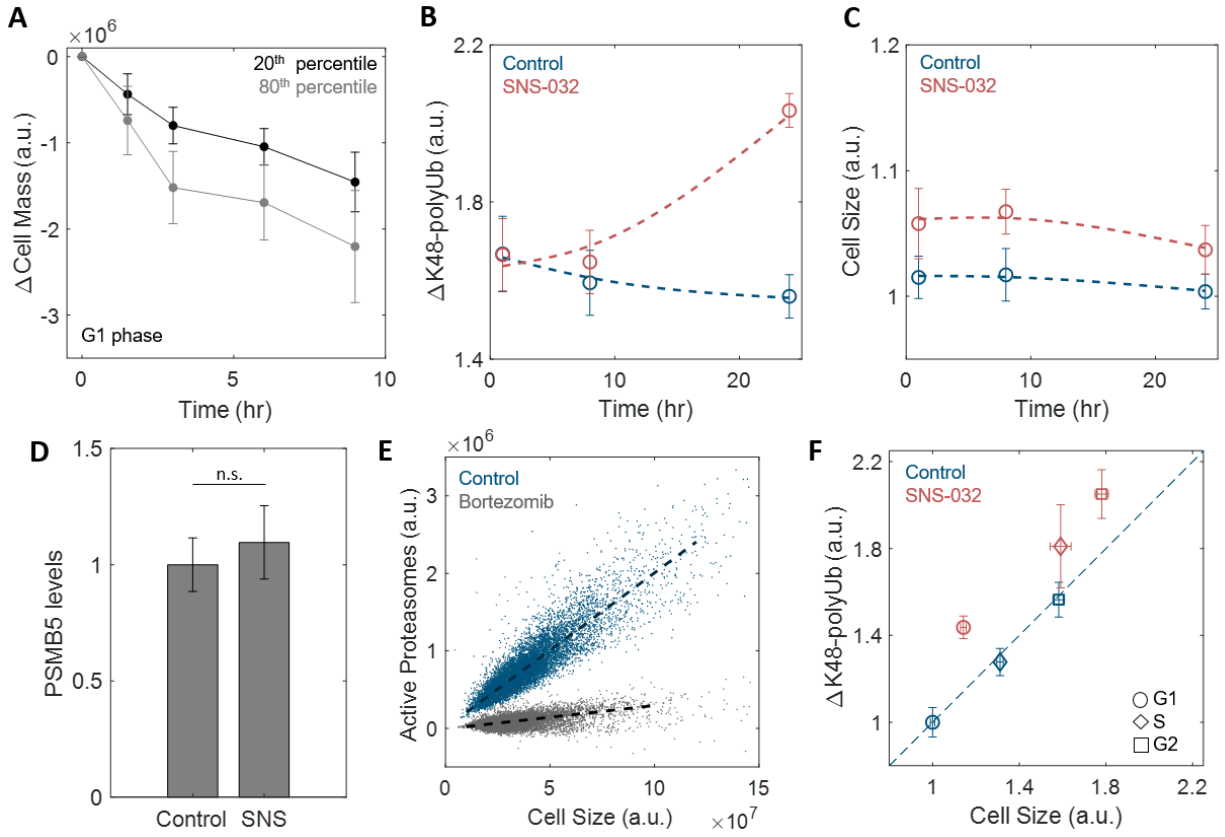

Figure 3. Large cells have higher rates of global protein degradation.
(A) Change in cell mass for small (20th percentile) or large (80th percentile) G1 cells following treatment with 10 μM cycloheximide, compared to time point 0 (0.1% v/v DMSO). Data presented as mean ± 95% confidence interval, n=5. **(B)** Clearance of K48-polyUb (ΔK48-polyUb, difference between levels of K48-polyUB in CFZ-treated (8 μM, 30 min) and corresponding non-CFZ-treated condition) and **(C)** cell size for control (0.1% v/v DMSO) or cells treated with 25 nM SNS-032 for 1, 8, or 24 hr. Data presented as median ± 95% confidence interval, n=9. Lines show smoothing spline fit. **(D)** Quantification of PSMB5 concentrations from 6 replicates of Western blots (see Fig. S4), presented as fold change of control. Data presented as mean ± SEM. **(E)** Single cell measurements of proteasome activity (MV151) as a function of cell size for control (0.1% v/v DMSO) and bortezomib-treated (1 μM) cells. Note the level of active proteasomes may be negative as the quantification was performed after subtraction of background noise. Lines show linear fit. **(F)** ΔK48-polyUb as a function of cell size for control or cells treated with 25 nM SNS-032 for 24 hr, separated by cell cycle stage. Values are normalized to the average of control G1 cells. Data presented as median ± 95% confidence interval, n=9. Dashed line represents proportional changes in ΔK48-polyUb and cell size (y=x). Note the proportional changes in ΔK48-polyUb and size for control and disproportional increase in ΔK48-polyUb compared to size for SNS-032 treated cells.

bioRxiv preprint doi: https://doi.org/10.1101/2021.11.09.467936; this version posted November 11, 2021. The copyright holder for this preprint (which was not certified by peer review) is the author/funder, who has granted bioRxiv a license to display the preprint in perpetuity. It is made available under aCC-BY-NC-ND 4.0 International license.

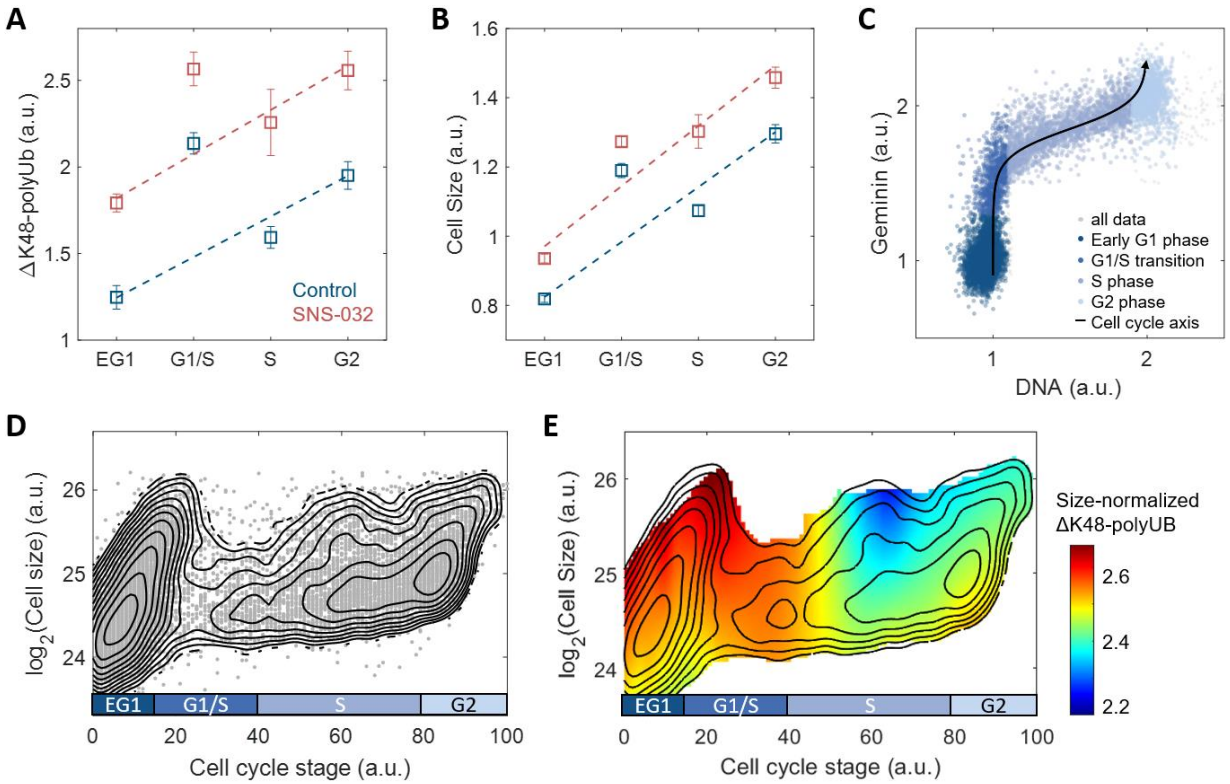

Figure 4. Hyperactivation of global protein degradation in large cells at the G1/S transition.

(A) Clearance of K48-polyUb (ΔK48-polyUb) and **(B)** cell size for control (0.1% v/v DMSO) or cells treated with 25 nM SNS-032, separated by cell cycle stage. Data presented as median ± 95% confidence interval, n=9. Lines show linear fit, excluding G1/S data, which deviates from the trend defined by G1, S, G2 cells. **(C)** Single cell measurements of DNA content (DAPI) and Geminin (mAG-hGem) in an unsynchronized population of proliferating RPE1 cells. Black curve represents an average cell cycle trajectory, which is used to parameterize the progression through the cell cycle and reduce the 2D DNA/Geminin representation into a 1D curve used in (D-E) (see Methods). **(D)** Single cell measurements of cell size (presented on logarithmic scale) as a function of cell cycle trajectory (see (C) and Methods) demonstrated in a scatterplot, overlayed with black contour lines representing the calculated joint probability density function, which describes the frequency of cells for every given paired value of cell size and cell cycle stage. **(E)** Heatmap of size-normalized ΔK48-polyUb (see Methods) overlaid on the contour lines from (D). See Fig.S6 for unnormalized ΔK48-polyUb.

bioRxiv preprint doi: https://doi.org/10.1101/2021.11.09.467936; this version posted November 11, 2021. The copyright holder for this preprint (which was not certified by peer review) is the author/funder, who has granted bioRxiv a license to display the preprint in perpetuity. It is made available under aCC-BY-NC-ND 4.0 International license.

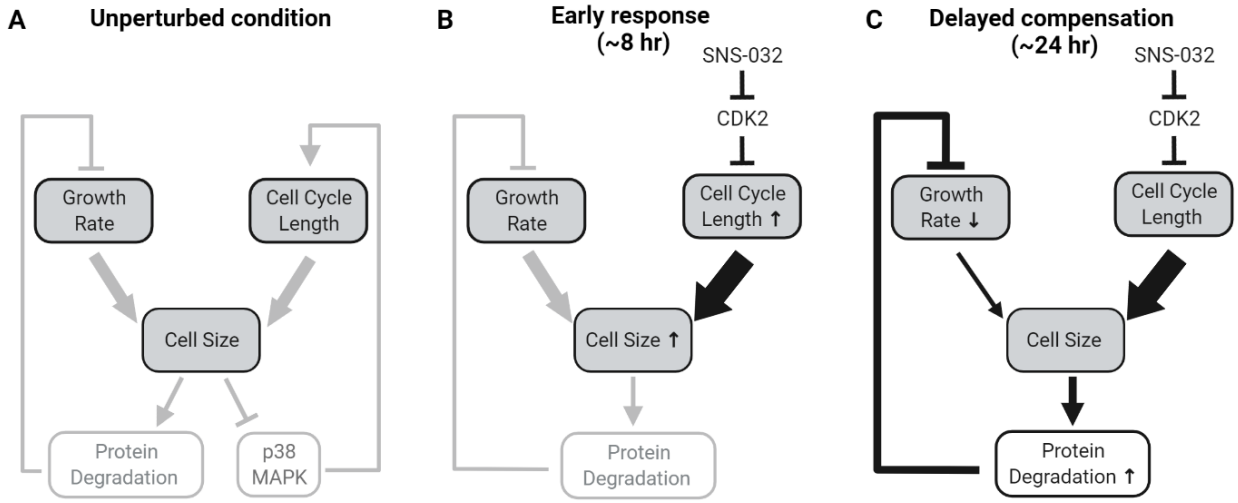

Figure 5. A model of size homeostatic control through compensatory degradation in large cells. (A) Control of cell size homeostasis involves negative feedback on both cell cycle duration and cellular growth rate. **(B)** Following CDK2 inhibition by SNS-032, cells undergo a longer cell cycle, contributing to an increase in cell size. **(C)** The large cell size following CDK2 inhibition then activates a delayed compensation through proteasome-mediated global protein degradation to restore cell size homeostasis. Gray arrows denote processes occurring at basal levels while black arrows demonstrate changes following the drug (SNS-032) perturbation.

bioRxiv preprint doi: https://doi.org/10.1101/2021.11.09.467936; this version posted November 11, 2021. The copyright holder for this preprint (which was not certified by peer review) is the author/funder, who has granted bioRxiv a license to display the preprint in perpetuity. It is made available under aCC-BY-NC-ND 4.0 International license.

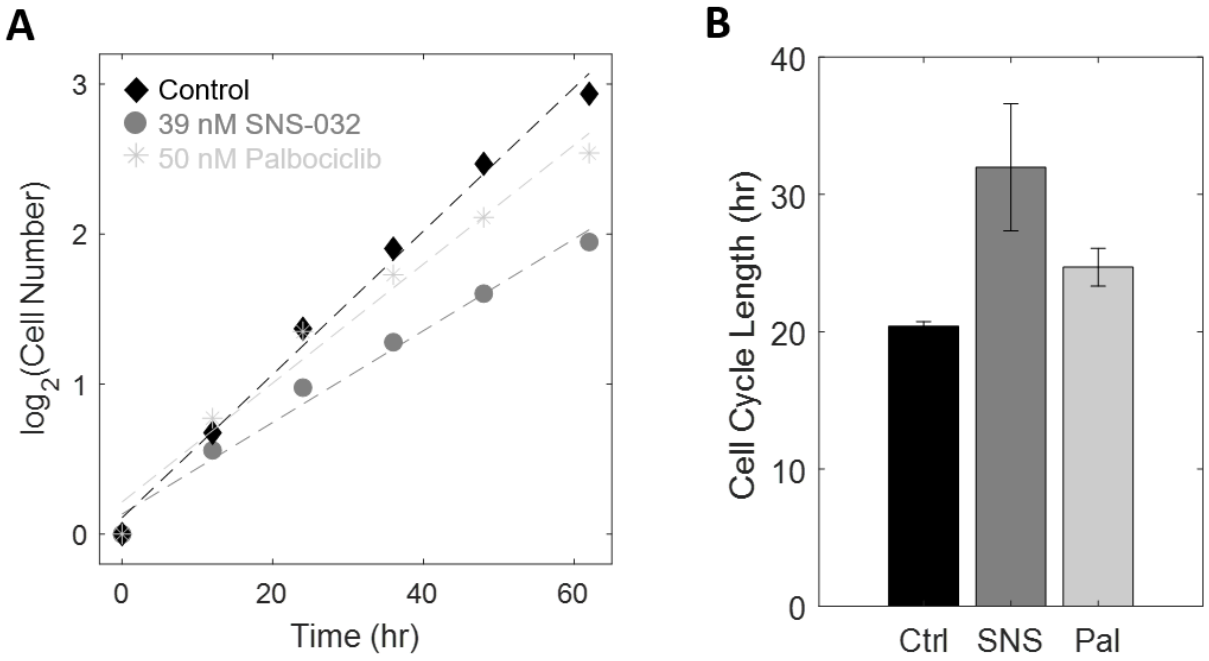

Supplementary Figure 1. Cells proliferate slower but maintain exponential proliferation under treatment of CDK2 and CDK4 inhibitors at the concentrations used.
(A) Exponential proliferation is shown as a linear trend between cell number (in log scale) over time for control (0.1% v/v DMSO), 39 nM SNS-032, and 50 nM palbociclib-treated cells. **(B)** Bar plot showing average cell cycle lengths for control, SNS-032, and palbociclib-treated cells. Data presented as mean ± SEM, n=3. Each condition is represented by measurements from a population of >5000 cells

bioRxiv preprint doi: https://doi.org/10.1101/2021.11.09.467936; this version posted November 11, 2021. The copyright holder for this preprint (which was not certified by peer review) is the author/funder, who has granted bioRxiv a license to display the preprint in perpetuity. It is made available under aCC-BY-NC-ND 4.0 International license.

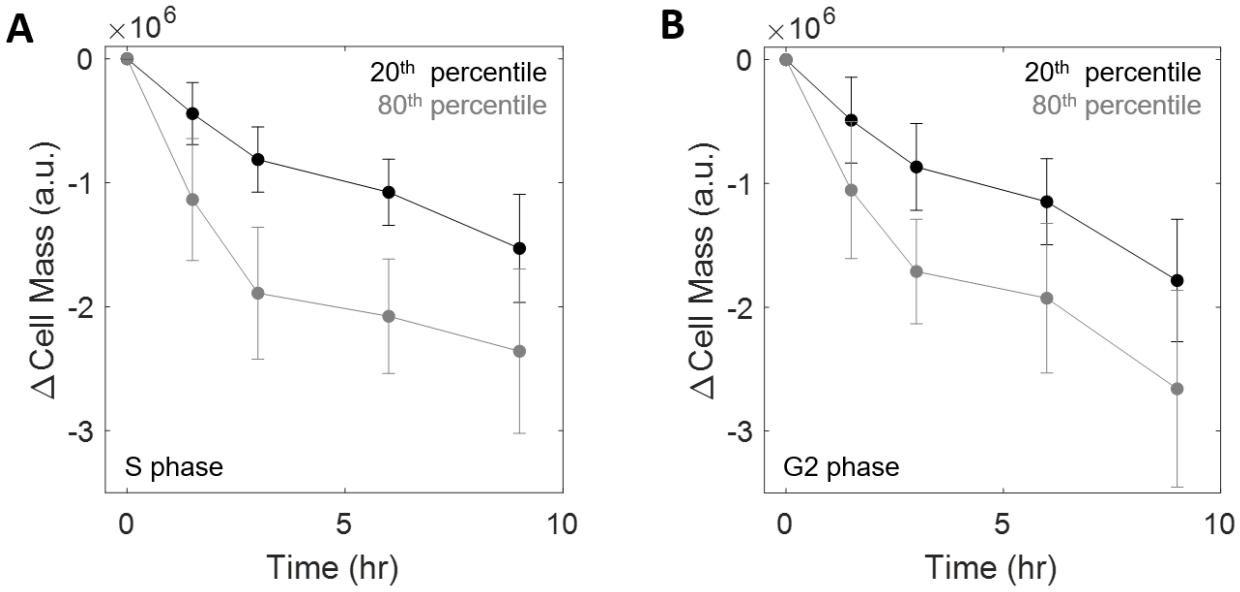

Supplementary Figure 2. Large cells show increased protein degradation throughout the cell cycle.

(A-B) Change in cell mass for small (20th percentile) or large (80th percentile) cells following treatment with 10 μM cycloheximide, in S (A) or G2 phase (B), compared to time point 0 (0.1% v/v DMSO). Data presented as mean ± 95% confidence interval, n=5. See Fig. 3A for cells in G1 phase.

bioRxiv preprint doi: https://doi.org/10.1101/2021.11.09.467936; this version posted November 11, 2021. The copyright holder for this preprint (which was not certified by peer review) is the author/funder, who has granted bioRxiv a license to display the preprint in perpetuity. It is made available under aCC-BY-NC-ND 4.0 International license.

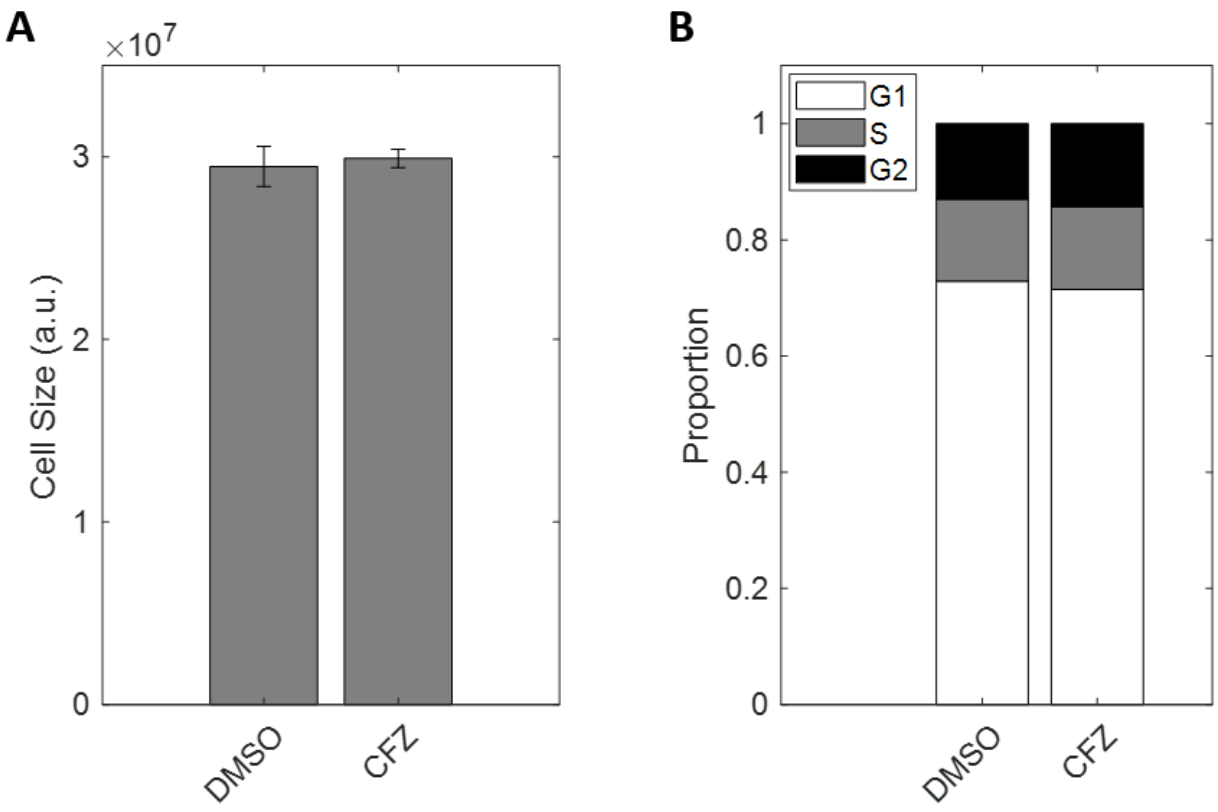

Supplementary Figure 3. Short treatment of the proteasome inhibitor CFZ does not affect cell size or fraction of cells in different cell cycle stages.

(A-B) Bar plots showing cell size (A) or fraction of cells in G1, S and G2 phase (B) of control (0.1% v/v DMSO) or cells treated with 30 min of 8 µM Carfilzomib (CFZ). Data presented as median ± 95% confidence interval, n=9.

bioRxiv preprint doi: https://doi.org/10.1101/2021.11.09.467936; this version posted November 11, 2021. The copyright holder for this preprint (which was not certified by peer review) is the author/funder, who has granted bioRxiv a license to display the preprint in perpetuity. It is made available under aCC-BY-NC-ND 4.0 International license.

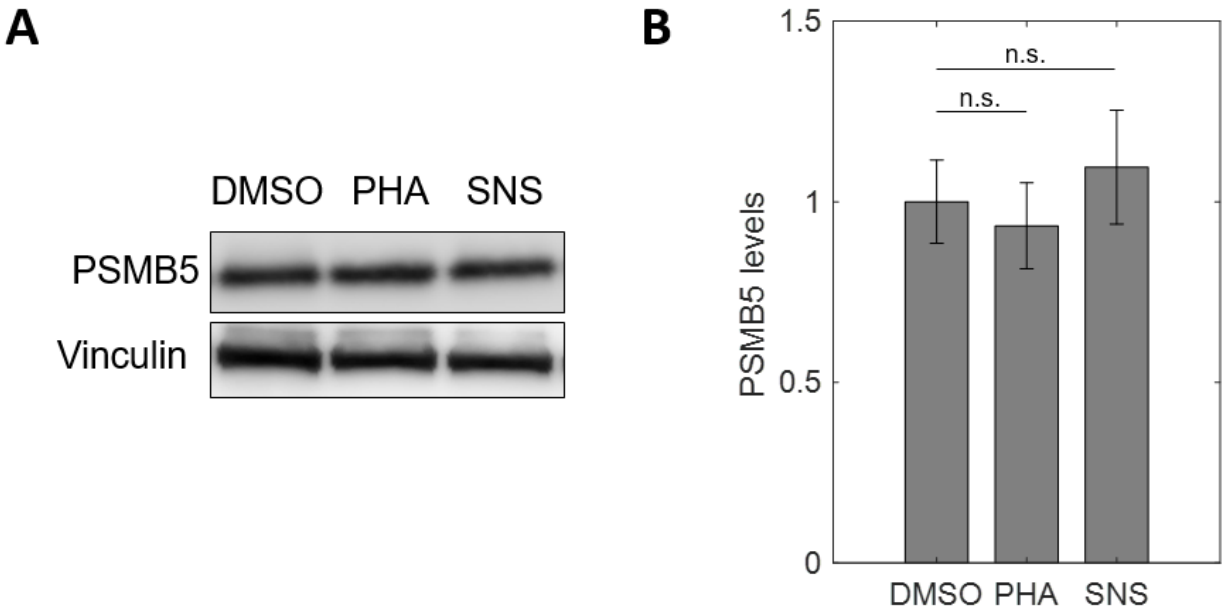

Supplementary Figure 4. CDK2 inhibition does not significantly affect proteasome content per unit mass.

(**A**) Western blots of cells under CDK2 inhibition through 44 hr of either 175 nM PHA848125 (PHA) or 39 nM SNS-032 (SNS) treatment. Note that Western blots lanes were loaded with lysates of equal protein. Vinculin is shown as a loading control. (**B**) Quantification of PSMB5 levels from 6 replicates of Western blots, presented as fold change of control. Data presented as mean ± SEM.

bioRxiv preprint doi: https://doi.org/10.1101/2021.11.09.467936; this version posted November 11, 2021. The copyright holder for this preprint (which was not certified by peer review) is the author/funder, who has granted bioRxiv a license to display the preprint in perpetuity. It is made available under aCC-BY-NC-ND 4.0 International license.

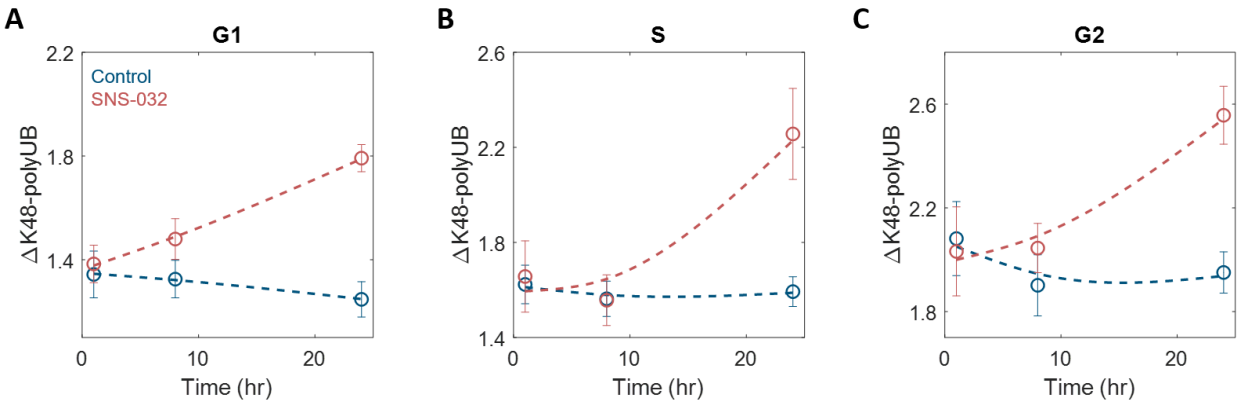

Supplementary Figure 5. CDK2 inhibition increases K48-polyUb turnover across cell cycle stages.

(A-C) Clearance of K48-polyUb (ΔK48-polyUb) for control or SNS-032 (25 nM) treated cells in G1 (A), S (B), or G2 (C) phase at 1, 8, or 24 hr of treatment. Data presented as median ± 95% confidence interval, n=9. Lines show smoothing spline fit.

bioRxiv preprint doi: https://doi.org/10.1101/2021.11.09.467936; this version posted November 11, 2021. The copyright holder for this preprint (which was not certified by peer review) is the author/funder, who has granted bioRxiv a license to display the preprint in perpetuity. It is made available under aCC-BY-NC-ND 4.0 International license.

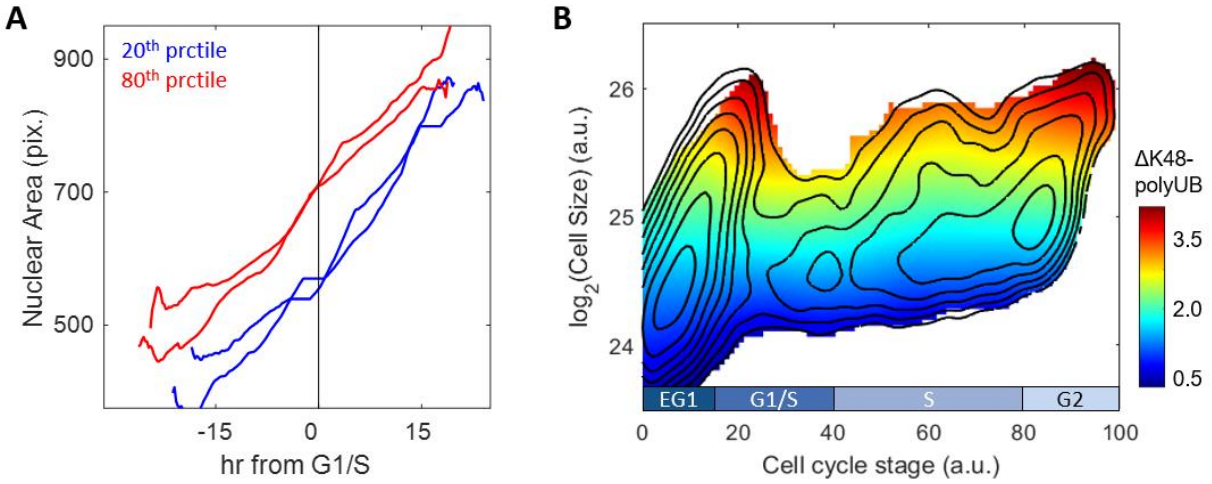

Supplementary Figure 6. Large cells prior to the G1/S transition continue through the cell cycle and show elevated ΔK48-polyUb.

(A) Example single-cell trajectories of nuclear area for small (20th percentile) and large (80th percentile) cells chosen ~2.5 hr before G1/S. Trajectories are smoothed with a moving average filter. **(B)** Heatmap of ΔK48-polyUb (see Methods) overlaid on the contour lines from Fig. 4D.

bioRxiv preprint doi: https://doi.org/10.1101/2021.11.09.467936; this version posted November 11, 2021. The copyright holder for this preprint (which was not certified by peer review) is the author/funder, who has granted bioRxiv a license to display the preprint in perpetuity. It is made available under aCC-BY-NC-ND 4.0 International license.

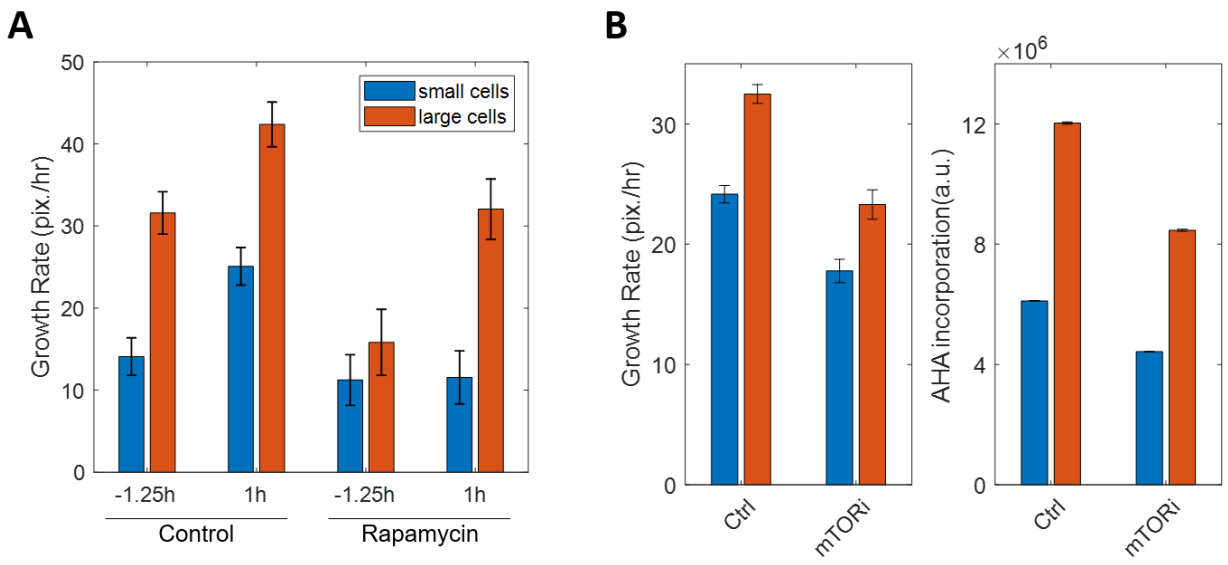

Supplementary Figure 7. Large cells prior to the G1/S transition show hyperactivated global protein degradation as demonstrated by live-cell imaging.
(A) Average growth rate of nuclear area for control (0.1% v/v DMSO, N=2724) or 5 nM rapamycin-treated cells (N=1172) at 1.25 hr before or 1 hr after the G1/S transition, separately shown for the small (30th percentile) and large (70th percentile) cells. Data presented as median ± 95% confidence interval. **(B)** Average growth rate of nuclear area and rates of protein synthesis for control and mTOR-inhibited (rapamycin for growth rate plots; torin2 for AHA incorporation plots) cells. Data presented as median ± 95% confidence interval.

bioRxiv preprint doi: https://doi.org/10.1101/2021.11.09.467936; this version posted November 11, 2021. The copyright holder for this preprint (which was not certified by peer review) is the author/funder, who has granted bioRxiv a license to display the preprint in perpetuity. It is made available under aCC-BY-NC-ND 4.0 International license.

References

Acebron, S.P., Karaulanov, E., Berger, B.S., Huang, Y.-L., and Niehrs, C. (2014). Mitotic wnt signaling promotes protein stabilization and regulates cell size. Mol. Cell *54*, 663–674.

Alber, A.B., and Suter, D.M. (2019). Dynamics of protein synthesis and degradation through the cell cycle. Cell Cycle *18*, 784–794.

Asadullah, Kumar, S., Saxena, N., Sarkar, M., Barai, A., and Sen, S. (2021). Combined heterogeneity in cell size and deformability promotes cancer invasiveness. J. Cell Sci. *134*.

Barr, A.R., Heldt, F.S., Zhang, T., Bakal, C., and Novák, B. (2016). A dynamical framework for the all-or-none G1/S transition. Cell Syst. *2*, 27–37.

Bell, C.D., and Waizbard, E. (1986). Variability of cell size in primary and metastatic human breast carcinoma. Invasion Metastasis *6*, 11–20.

Berenson, D.F., Zatulovskiy, E., Xie, S., and Skotheim, J.M. (2019). Constitutive expression of a fluorescent protein reports the size of live human cells. Mol. Biol. Cell *30*, 2985–2995.

Boehlke, C., Kotsis, F., Patel, V., Braeg, S., Voelker, H., Bredt, S., Beyer, T., Janusch, H., Hamann, C., Gödel, M., et al. (2010). Primary cilia regulate mTORC1 activity and cell size through Lkb1. Nat. Cell Biol. *12*, 1115–1122.

Cadart, C., Monnier, S., Grilli, J., Sáez, P.J., Srivastava, N., Attia, R., Terriac, E., Baum, B., Cosentino-Lagomarsino, M., and Piel, M. (2018). Size control in mammalian cells involves modulation of both growth rate and cell cycle duration. Nat. Commun. *9*, 3275.

Calve, S., Witten, A.J., Ocken, A.R., and Kinzer-Ursem, T.L. (2016). Incorporation of non-canonical amino acids into the developing murine proteome. Sci. Rep. *6*, 32377.

Cheng, L., Chen, J., Kong, Y., Tan, C., Kafri, R., and Bjorklund, M. (2021). Size-scaling promotes senescence-like changes in proteome and organelle content. bioRxiv.

Collins, G.A., and Goldberg, A.L. (2017). The Logic of the 26S Proteasome. Cell *169*, 792–806.

D'Ario, M., Tavares, R., Schiessl, K., Desvoyes, B., Gutierrez, C., Howard, M., and Sablowski, R. (2021). Cell size controlled in plants using DNA content as an internal scale. Science *372*, 1176–1181.

Dhawan, S., Georgia, S., and Bhushan, A. (2007). Formation and regeneration of the endocrine pancreas. Curr. Opin. Cell Biol. *19*, 634–645.

Dolznig, H., Grebien, F., Sauer, T., Beug, H., and Müllner, E.W. (2004). Evidence for a size-sensing mechanism in animal cells. Nat. Cell Biol. *6*, 899–905.

Franklin, J.L., and Johnson, E.M. (1998). Control of Neuronal Size Homeostasis by Trophic Factor–mediated Coupling of Protein Degradation to Protein Synthesis. J. Cell Biol. *142*, 1313–1324.

Ghenim, L., Allier, C., Obeid, P., Hervé, L., Fortin, J.-Y., Balakirev, M., and Gidrol, X. (2021). A new ultradian rhythm in mammalian cell dry mass observed by holography. Sci. Rep. *11*, 1290.

bioRxiv preprint doi: https://doi.org/10.1101/2021.11.09.467936; this version posted November 11, 2021. The copyright holder for this preprint (which was not certified by peer review) is the author/funder, who has granted bioRxiv a license to display the preprint in perpetuity. It is made available under aCC-BY-NC-ND 4.0 International license.

Ginzberg, M.B., Kafri, R., and Kirschner, M. (2015). Cell biology. On being the right (cell) size. Science *348*, 1245075.

Ginzberg, M.B., Chang, N., D'Souza, H., Patel, N., Kafri, R., and Kirschner, M.W. (2018). Cell size sensing in animal cells coordinates anabolic growth rates and cell cycle progression to maintain cell size uniformity. eLife *7*.

Gordon, B.S., Kelleher, A.R., and Kimball, S.R. (2013). Regulation of muscle protein synthesis and the effects of catabolic states. Int. J. Biochem. Cell Biol. *45*, 2147–2157.

Hartwell, L.H., Culotti, J., Pringle, J.R., and Reid, B.J. (1974). Genetic control of the cell division cycle in yeast. Science *183*, 46–51.

Helman, A., Klochendler, A., Azazmeh, N., Gabai, Y., Horwitz, E., Anzi, S., Swisa, A., Condiotti, R., Granit, R.Z., Nevo, Y., et al. (2016). p16(Ink4a)-induced senescence of pancreatic beta cells enhances insulin secretion. Nat. Med. *22*, 412–420.

Johnston, G., Pringle, J., and Hartwell, L. (1977). Coordination of growth with cell division in the yeast. Experimental Cell Research *105*, 79–98.

Kafri, R., Levy, J., Ginzberg, M.B., Oh, S., Lahav, G., and Kirschner, M.W. (2013). Dynamics extracted from fixed cells reveal feedback linking cell growth to cell cycle. Nature *494*, 480–483.

Karin, O., Raz, M., Tendler, A., Bar, A., Korem Kohanim, Y., Milo, T., and Alon, U. (2020). A new model for the HPA axis explains dysregulation of stress hormones on the timescale of weeks. Mol. Syst. Biol. *16*, e9510.

Karin, O., Raz, M., and Alon, U. (2021). An opponent process for alcohol addiction based on changes in endocrine gland mass. iScience *24*, 102127.

Killander, D., and Zetterberg, A. (1965). A quantitative cytochemical investigation of the relationship between cell mass and initiation of DNA synthesis in mouse fibroblasts in vitro. Exp. Cell Res. *40*, 12–20.

Lanz, M.C., Zatulovskiy, E., Swaffer, M.P., Zhang, L., and Zhang, S. (2021). Increasing cell size remodels the proteome and promotes senescence. bioRxiv.

Lecker, S.H., Goldberg, A.L., and Mitch, W.E. (2006). Protein Degradation by the Ubiquitin–Proteasome Pathway in Normal and Disease States. J. Am. Soc. Nephrol. *17*, 1807–1819.

Lee, S.-H., Park, Y., Yoon, S.K., and Yoon, J.-B. (2010). Osmotic stress inhibits proteasome by p38 MAPK-dependent phosphorylation. J. Biol. Chem. *285*, 41280–41289.

Lee, T.K., Esinhart, J.D., Blackburn, L.D., and Silverman, J.F. (1992). The size of small cell lung carcinoma cells. Ratio to lymphocytes and correlation with specimen size and crush artifact. Anal. Quant. Cytol. Histol. *14*, 32–34.

Leestemaker, Y., de Jong, A., Witting, K.F., Penning, R., Schuurman, K., Rodenko, B., Zaal, E.A., van de Kooij, B., Laufer, S., Heck, A.J.R., et al. (2017). Proteasome Activation by Small Molecules. Cell Chem Biol *24*, 725–736.e7.

Liu, S., Ginzberg, M.B., Patel, N., Hild, M., Leung, B., Li, Z., Chen, Y.-C., Chang, N., Wang, Y., Tan, C., et al. (2018). Size uniformity of animal cells is actively maintained by a p38 MAPK-

bioRxiv preprint doi: https://doi.org/10.1101/2021.11.09.467936; this version posted November 11, 2021. The copyright holder for this preprint (which was not certified by peer review) is the author/funder, who has granted bioRxiv a license to display the preprint in perpetuity. It is made available under aCC-BY-NC-ND 4.0 International license.

dependent regulation of G1-length. Elife *7*.

Liu, X., Oh, S., Peshkin, L., and Kirschner, M.W. (2020). Computationally enhanced quantitative phase microscopy reveals autonomous oscillations in mammalian cell growth. Proc. Natl. Acad. Sci. U. S. A. *117*, 27388–27399.

Livneh, I., Cohen-Kaplan, V., Cohen-Rosenzweig, C., Avni, N., and Ciechanover, A. (2016). The life cycle of the 26S proteasome: from birth, through regulation and function, and onto its death. Cell Res. *26*, 869–885.

Miettinen, T.P., Pessa, H.K.J., Caldez, M.J., Fuhrer, T., Diril, M.K., Sauer, U., Kaldis, P., and Björklund, M. (2014). Identification of transcriptional and metabolic programs related to mammalian cell size. Curr. Biol. *24*, 598–608.

Mitchison, J.M. (1971). The Biology of the Cell Cycle (CUP Archive).

Mugahid, D., Kalocsay, M., Liu, X., Gruver, J.S., Peshkin, L., and Kirschner, M.W. (2020). YAP regulates cell size and growth dynamics via non-cell autonomous mediators. Elife *9*.

Nakayama, K.I., and Nakayama, K. (2006). Ubiquitin ligases: cell-cycle control and cancer. Nat. Rev. Cancer *6*, 369–381.

Neufeld, T.P., de la Cruz, A.F., Johnston, L.A., and Edgar, B.A. (1998). Coordination of growth and cell division in the Drosophila wing. Cell *93*, 1183–1193.

Neurohr, G.E., Terry, R.L., Lengefeld, J., Bonney, M., Brittingham, G.P., Moretto, F., Miettinen, T.P., Vaites, L.P., Soares, L.M., Paulo, J.A., et al. (2019). Excessive Cell Growth Causes Cytoplasm Dilution And Contributes to Senescence. Cell *176*, 1083–1097.e18.

Nurse, P. (1975). Genetic control of cell size at cell division in yeast. Nature *256*, 547–551.

Rojas-Canales, D.M., Li, J.Y., Makuei, L., and Gleadle, J.M. (2019). Compensatory renal hypertrophy following nephrectomy: When and how? Nephrology *24*, 1225–1232.

Russell, S.J., Steger, K.A., and Johnston, S.A. (1999). Subcellular localization, stoichiometry, and protein levels of 26 S proteasome subunits in yeast. J. Biol. Chem. *274*, 21943–21952.

Sakaue-Sawano, A., Kurokawa, H., Morimura, T., Hanyu, A., Hama, H., Osawa, H., Kashiwagi, S., Fukami, K., Miyata, T., Miyoshi, H., et al. (2008). Visualizing spatiotemporal dynamics of multicellular cell-cycle progression. Cell *132*.

Sandri, M. (2013). Protein breakdown in muscle wasting: role of autophagy-lysosome and ubiquitin-proteasome. Int. J. Biochem. Cell Biol. *45*, 2121–2129.

Schmoller, K.M., Turner, J.J., Kõivomägi, M., and Skotheim, J.M. (2015). Dilution of the cell cycle inhibitor Whi5 controls budding-yeast cell size. Nature *526*, 268–272.

Sellam, A., Chaillot, J., Mallick, J., Tebbji, F., Richard Albert, J., Cook, M.A., and Tyers, M. (2019). The p38/HOG stress-activated protein kinase network couples growth to division in Candida albicans. PLoS Genet. *15*, e1008052.

Serrano-Mislata, A., Schiessl, K., and Sablowski, R. (2015). Active Control of Cell Size Generates Spatial Detail during Plant Organogenesis. Curr. Biol. *25*, 2991–2996.

bioRxiv preprint doi: https://doi.org/10.1101/2021.11.09.467936; this version posted November 11, 2021. The copyright holder for this preprint (which was not certified by peer review) is the author/funder, who has granted bioRxiv a license to display the preprint in perpetuity. It is made available under aCC-BY-NC-ND 4.0 International license.

Son, S., Tzur, A., Weng, Y., Jorgensen, P., Kim, J., Kirschner, M.W., and Manalis, S.R. (2012). Direct observation of mammalian cell growth and size regulation. Nat. Methods *9*, 910–912.

Tan, C., Ginzberg, M.B., Webster, R., Iyengar, S., Liu, S., Papadopoli, D., Concannon, J., Wang, Y., Auld, D.S., Jenkins, J.L., et al. (2021). Cell size homeostasis is maintained by CDK4-dependent activation of p38 MAPK. Dev. Cell *56*, 1756–1769.e7.

Varsano, G., Wang, Y., and Wu, M. (2017). Probing Mammalian Cell Size Homeostasis by Channel-Assisted Cell Reshaping. Cell Rep. *20*, 397–410.

Verdoes, M., Florea, B.I., Menendez-Benito, V., Maynard, C.J., Witte, M.D., van der Linden, W.A., van den Nieuwendijk, A.M.C.H., Hofmann, T., Berkers, C.R., van Leeuwen, F.W.B., et al. (2006). A fluorescent broad-spectrum proteasome inhibitor for labeling proteasomes in vitro and in vivo. Chem. Biol. *13*, 1217–1226.

Willis, L., Refahi, Y., Wightman, R., Landrein, B., Teles, J., Huang, K.C., Meyerowitz, E.M., and Jönsson, H. (2016). Cell size and growth regulation in the Arabidopsis thaliana apical stem cell niche. Proc. Natl. Acad. Sci. U. S. A. *113*, E8238–E8246.

Xie, S., and Skotheim, J.M. (2020). A G1 Sizer Coordinates Growth and Division in the Mouse Epidermis. Curr. Biol. *30*, 916–924.e2.

Yau, R., and Rape, M. (2016). The increasing complexity of the ubiquitin code. Nat. Cell Biol. *18*, 579–586.

Zatulovskiy, E., Zhang, S., Berenson, D.F., Topacio, B.R., and Skotheim, J.M. (2020). Cell growth dilutes the cell cycle inhibitor Rb to trigger cell division. Science *369*, 466–471.

Zetterberg, A., and Killander, D. (1965). Quantitative cytochemical studies on interphase growth. Experimental Cell Research *39*, 22–32.

Zinder, O., and Shapiro, B. (1971). Effect of cell size on epinephrine- and ACTH-induced fatty acid release from isolated fat cells. Journal of Lipid Research *12*, 91–95.